

# Observation of Localized Multi-Spatial-Mode Quadrature Squeezing

Embrey, Christopher; Turnbull, Matthew; Petrov, Plamen; Boyer, Vincent

DOI:

[10.1103/PhysRevX.5.031004](https://doi.org/10.1103/PhysRevX.5.031004)

License:

Creative Commons: Attribution (CC BY)

*Document Version*

Publisher's PDF, also known as Version of record

*Citation for published version (Harvard):*

Embrey, C, Turnbull, M, Petrov, P & Boyer, V 2015, 'Observation of Localized Multi-Spatial-Mode Quadrature Squeezing', *Physical Review X*, vol. 5, no. 3, 031004. <https://doi.org/10.1103/PhysRevX.5.031004>

[Link to publication on Research at Birmingham portal](#)

## **Publisher Rights Statement:**

This article is available under the terms of the Creative Commons Attribution 3.0 License. Further distribution of this work must maintain attribution to the author(s) and the published article's title, journal citation, and DOI.

Eligibility for repository checked July 2015

## **General rights**

Unless a licence is specified above, all rights (including copyright and moral rights) in this document are retained by the authors and/or the copyright holders. The express permission of the copyright holder must be obtained for any use of this material other than for purposes permitted by law.

- Users may freely distribute the URL that is used to identify this publication.
- Users may download and/or print one copy of the publication from the University of Birmingham research portal for the purpose of private study or non-commercial research.
- User may use extracts from the document in line with the concept of 'fair dealing' under the Copyright, Designs and Patents Act 1988 (?)
- Users may not further distribute the material nor use it for the purposes of commercial gain.

Where a licence is displayed above, please note the terms and conditions of the licence govern your use of this document.

When citing, please reference the published version.

## **Take down policy**

While the University of Birmingham exercises care and attention in making items available there are rare occasions when an item has been uploaded in error or has been deemed to be commercially or otherwise sensitive.

If you believe that this is the case for this document, please contact [UBIRA@lists.bham.ac.uk](mailto:UBIRA@lists.bham.ac.uk) providing details and we will remove access to the work immediately and investigate.

# Observation of Localized Multi-Spatial-Mode Quadrature Squeezing

C. S. Embrey,<sup>1</sup> M. T. Turnbull,<sup>1,2</sup> P. G. Petrov,<sup>1</sup> and V. Boyer<sup>1,\*</sup>

<sup>1</sup>*Midlands Ultracold Atom Research Centre, School of Physics and Astronomy, University of Birmingham, Edgbaston, Birmingham B15 2TT, United Kingdom*

<sup>2</sup>*Gravitational Research Group, Physics Department, John Anderson Building, University of Strathclyde, Glasgow G4 0NG, United Kingdom*

(Received 19 September 2014; revised manuscript received 27 February 2015; published 9 July 2015)

Quantum states of light can improve imaging whenever the image quality and resolution are limited by the quantum noise of the illumination. In the case of a bright illumination, quantum enhancement is obtained for a light field composed of many squeezed transverse modes. A possible realization of such a multi-spatial-mode squeezed state is a field which contains a transverse plane in which the local electric field displays reduced quantum fluctuations at all locations, on any one quadrature. Using a traveling-wave amplifier, we have generated a multi-spatial-mode squeezed state and showed that it exhibits localized quadrature squeezing at any point of its transverse profile, in regions much smaller than its size. We observe 75 independently squeezed regions. The amplification relies on nondegenerate four-wave mixing in a hot vapor and produces a bichromatic squeezed state. The result confirms the potential of this technique for producing illumination suitable for practical quantum imaging.

DOI: [10.1103/PhysRevX.5.031004](https://doi.org/10.1103/PhysRevX.5.031004)

Subject Areas: Optics, Photonics, Quantum Physics

## I. INTRODUCTION

When performed with a classical light source, optical measurements are limited by the quantum fluctuations of the electromagnetic field, which produce noise at the so-called quantum-noise level (QNL). It is, however, possible to improve on the QNL using quantum states of light, for instance, squeezed light [1]. To be useful for full-field-of-view imaging applications, a quantum state of light must be spatially multimode, so that it can probe or carry spatial information [2]. Recently, there has been substantial progress in few-photon quantum imaging techniques, where the illumination is very low and the photons are detected individually. These few-photon entangled states have yielded clearer images than those produced by the equivalent classical illuminations, whose QNL-limited signal-to-noise ratios are nominally poor. In particular, these states have produced images of amplitude [3] and phase [4,5] objects with noise below the QNL, and interferences displaying better spatial resolution [6]. These experiments do not rely on the ability of generating a high level of quadrature squeezing, which remains usually very low, but rather on the possibility of generating a few photon pairs with a good fidelity using low-gain parametric down-conversion in a nonlinear crystal.

Although very low-level illumination may be required in select applications, there is a broader interest in applying quantum imaging techniques to the cases where a bright illumination can be applied. In this case, the signal-to-noise ratio at the QNL is much higher, and quantum light, specifically quadrature-squeezed light, can provide an improvement over an already optimized classical detection. Unlike for the few-photon illumination, quantum-noise reduction with bright illumination is achieved using strong quadrature squeezing.

The benefit of squeezed light to determine the position of a fixed particle has already been demonstrated in a biological environment with a single squeezed mode [7]. Quantum-enhanced imaging of a more complex object can also be achieved by squeezing the relevant mode in optical scanning microscopy techniques [8]. However, improving the spatial resolution in a single-shot imaging of the full field of view would require a multi-spatial-mode (MSM) quadrature-squeezed light field [9]. While efficient multimode generation of squeezed light has been reported in optical parametric oscillators in the time domain [10,11], the realization of quadrature squeezing in a large number of spatial modes has remained a long-standing goal in the field of quantum optics [12]. The main hurdle in the generation of MSM-squeezed light has been the lack of an available strong multimode nonlinearity. Enhancing weak nonlinearities in  $\chi^{(2)}$  crystals with a spatially degenerate cavity is feasible [13] and, in principle, scalable, but success has been limited to a small number of spatial modes [14]. A possible solution is to operate without a cavity in a pulsed regime, where large peak pump intensities lead to large levels of squeezing. However, this approach has been

\*v.boyer@bham.ac.uk

*Published by the American Physical Society under the terms of the Creative Commons Attribution 3.0 License. Further distribution of this work must maintain attribution to the author(s) and the published article's title, journal citation, and DOI.*

limited to producing correlations between twin beams (two-mode squeezed state) [15–17] rather than producing a single squeezed beam. Another workaround is the direct engineering of overlapping squeezed modes [18], but practical scalability is also lacking.

An alternative to parametric down-conversion is the large resonant  $\chi^{(3)}$  atomic nonlinearities that have been shown to be promising alternatives for the production of quantum field correlations in the spatial domain [19,20]. In this paper, we report on using such nondegenerate four-wave mixing (4WM) in a hot vapor as a large-gain multimode amplifier. This has allowed us to generate a vacuum which is quadrature squeezed in a large number of spatial modes. In particular, we have demonstrated localized vacuum quadrature squeezing, in a configuration which, when superimposed to a bright coherent state, would be suitable for enhanced optical resolution applications.

## II. BACKGROUND

In free space, an optical mode is described quantum mechanically by the field quadrature operators  $X$  and  $Y$ . The noncommutativity of  $X$  and  $Y$  implies a Heisenberg inequality  $\Delta X \Delta Y \geq \frac{1}{4}$  which is responsible for the quantum fluctuations of the electromagnetic field. The QNL is reached when the inequality is saturated—it then describes a so-called minimum uncertainty state—and the uncertainties on both quadratures are equal. It is possible to reduce, or “squeeze,” the uncertainty on one of the quadratures below the QNL, as long as it is compensated by an equal increase on the other quadrature.

To illustrate the key signature of a MSM-squeezed state, let us first consider the homodyne detection of a single-mode squeezed state. In such a configuration, a bright local oscillator (LO) beats with the squeezed mode and amplifies the fluctuations of one of its quadratures [Fig. 1(a)]. Because the LO selects the spatial mode to be analyzed, it is important to achieve a good overlap between the optical modes of the LO and the squeezed field. Soon after the first observation of squeezed light [21], the question of

“local” squeezing was raised [12], that is to say, the possibility of generating and observing a light field with reduced quantum fluctuations at any point of its transverse profile. Equivalently, such a field would display quadrature squeezing on a homodyne detector operated with an arbitrary spatial configuration of the LO [22], as depicted in Fig. 1(b). This MSM quadrature-squeezed field has been theoretically shown to allow an improvement of the spatial resolution beyond the QNL in certain schemes of optical super-resolution [9], but its efficient generation has remained elusive until the present work.

To describe more formally the properties of a MSM-squeezed state, let us consider a light field propagating along the  $z$  axis, in a minimum uncertainty state, such that in the near field ( $z = 0$ ), the  $Y$  quadrature is squeezed at all points  $\boldsymbol{\rho}$  in the transverse plane:  $\Delta Y(\boldsymbol{\rho}) < \frac{1}{2}$ . Classically, and in the Fraunhofer diffraction limit, the transverse distribution of the far electric field at  $z = \infty$  is the Fourier transform  $E(\mathbf{q})$  of the transverse distribution  $E(\boldsymbol{\rho})$  of the near electric field. Quantum mechanically, this property results in quantum correlations in the far field between positions  $\mathbf{q}$  and  $-\mathbf{q}$  due to the joint quadratures  $X_-(\mathbf{q}) = [X(\mathbf{q}) - X(-\mathbf{q})]/\sqrt{2}$  and  $Y_+(\mathbf{q}) = [Y(\mathbf{q}) + Y(-\mathbf{q})]/\sqrt{2}$  being squeezed for all  $\mathbf{q}$  (Appendix A).

Such a state can be created by a traveling-wave amplifier. This device creates Stokes and anti-Stokes fields (called twin beams, or probe and conjugate, or signal and idler) at the sideband frequencies  $-\Omega$  and  $\Omega$  with respect to a central frequency  $\omega_0$ , which classically fulfil the phase conjugation  $E(-\Omega) = E^*(\Omega)$  [23]. For a thin amplifier, diffraction during the propagation is negligible and the phase conjugation at the output retains its local character:  $E(\boldsymbol{\rho}, -\Omega) = E^*(\boldsymbol{\rho}, \Omega)$  for all  $\boldsymbol{\rho}$ . Quantum mechanically, this local phase conjugation translates into local quantum correlations in the near field (i.e., at the position where they are created in the amplifier). Specifically, the quantum fluctuations of the joint quadratures  $X_-(\boldsymbol{\rho}, \Omega) = [X(\boldsymbol{\rho}, \Omega) - X(\boldsymbol{\rho}, -\Omega)]/\sqrt{2}$  and  $Y_+(\boldsymbol{\rho}, \Omega) = [Y(\boldsymbol{\rho}, \Omega) + Y(\boldsymbol{\rho}, -\Omega)]/\sqrt{2}$  are reduced below the QNL, while the similarly defined joint quadratures  $X_+(\boldsymbol{\rho}, \Omega)$  and  $Y_-(\boldsymbol{\rho}, \Omega)$  are antisqueezed. When the probe and conjugate fields are degenerate, i.e., when  $\Omega = 0$ , this naturally leads the  $Y$  quadrature to be squeezed at dc in the near field.

The amount of squeezing is directly related to the thin amplifier gain. If the gain is too low, a resonant cavity can be used, provided it is spatially degenerate [13]. Experimentally, this proves challenging [14] and a large-gain traveling-wave amplifier may be preferable, for instance, a 4WM process in a hot atomic vapor [24].

This nonlinear atomic system has been used to demonstrate symmetric correlations in the far field; in a non-degenerate configuration, it gives rise to entangled images [25] while in a degenerate configuration it produces quadrature squeezing for centrally symmetric modes [20]. The

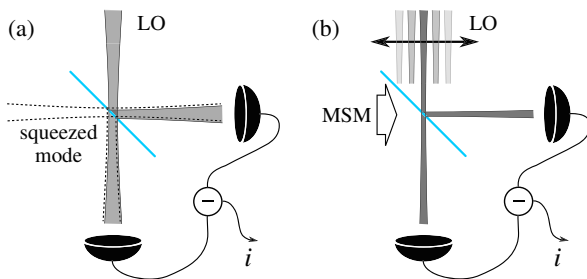


FIG. 1. The homodyne detection of a squeezed state leads to reduced noise on the balanced photocurrent  $i$  below the QNL. (a) For a single-spatial-mode squeezed state, the mode of the LO must match the squeezed mode. (b) For a hypothetical MSM squeezed state, the LO could have any shape or position.

local multimode operation of the device was also evidenced by noiseless amplification of near-field images [26]. Here, we report on the direct measurement of the local squeezing of a MSM-squeezed state using a homodyne detector with an arbitrarily shaped LO, as shown in Fig. 1(b).

### III. FOUR-WAVE MIXING AS A TRAVELING-WAVE AMPLIFIER

We use the  $D1$  line of rubidium 85 to generate probe and conjugate fields, using the 4WM scheme shown in Fig. 2 [24]. A single pump beam, at frequency  $\omega_0$ , couples a probe field, at frequency  $\omega_p = \omega_0 - \Omega$ , with a conjugate field, at frequency  $\omega_c = \omega_0 + \Omega$ , where  $\Omega$  is of the order of the ground-state hyperfine splitting (approximately 3 GHz). The process is efficient for a range of detunings  $\delta$  between the pump-probe Raman transition and the hyperfine splitting. This effectively sets the squeezing bandwidth  $\Delta\Omega$  to approximately 20 MHz.

The phase-matching condition, which requires the probe and conjugate fields to propagate symmetrically on opposite sides of the pump, is relaxed by the finite length of the rubidium cell. As a result, a large number of pairs of modes, propagating along slightly different directions, are coupled by the 4WM process [19,27]. Although the 4WM follows a copropagating configuration (forward 4WM), dispersion of the index of refraction induces a small angle between the pump axis and the direction of maximum probe gain [28]. The resulting far-field spatial gain profile (Fig. 3) shows that the spatial gain spectrum peaks for a finite value of  $|\mathbf{q}|$  and is reduced close to  $|\mathbf{q}| = 0$ . Consequently, the region of substantial gain forms an annulus due to the axial symmetry around the  $z$  axis (Fig. 4). The gap in the gain around  $|\mathbf{q}| = 0$  means that probe and conjugate modes with low transverse spatial frequencies are only weakly coupled by the 4WM process and cannot develop strong quantum correlations. To fix this shortcoming, we can use modes whose probe and conjugate spatial frequency spectra are each confined to opposite restricted gain regions (RGRs) of the gain annulus. These confined modes see a gapless effective gain spectrum in both the  $x$  and  $y$  directions for both their probe and conjugate components (Fig. 4).

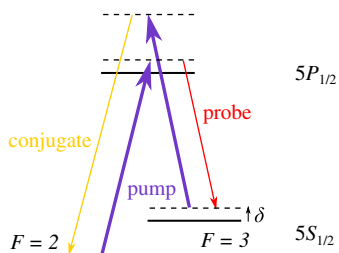


FIG. 2. Nondegenerate four-wave-mixing scheme on the  $D1$  line of  $^{85}\text{Rb}$ . A single pump field creates correlations between the probe and conjugate fields, whose frequencies are separated by roughly twice the ground-state hyperfine splitting.

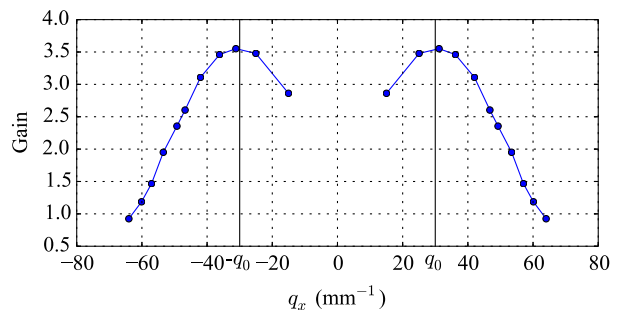


FIG. 3. Spatial gain spectrum as inferred from the spatial gain profile in the far field. The probe field is seeded with a Gaussian beam at a variable angle with the pump beam, and the ratio between the seed power and output probe power is measured. The profile has been measured along the  $x$  direction but would be the same along any radial direction. The gain at low  $q_x$  is not accurately measurable due to pump light leakage at  $q_x = 0$ .

In order to avoid the separate propagation of these restricted probe and conjugate modes, imposed by the phase-matching condition, we overlap on a beam splitter two correlated propagation axes ( $A_1$  and  $A_2$ ) corresponding to positions  $\pm\mathbf{q}_0$  in the far field. The direction of  $\mathbf{q}_0$  is arbitrarily chosen to be along the  $x$  radial direction, as

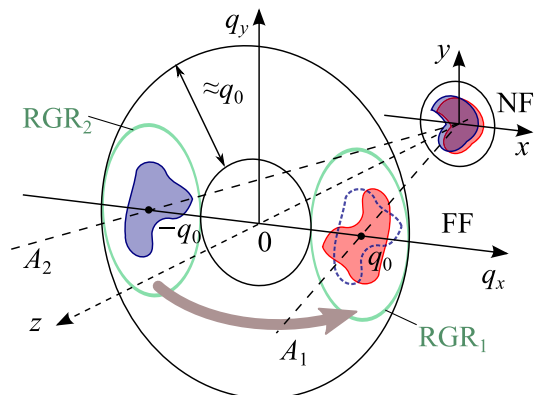


FIG. 4. Geometry of the localized squeezing preparation. A 4WM gain medium in the near field (NF) produces local quantum correlations between the  $\Omega$  and the  $-\Omega$  sidebands. As a result, overlapped modes fulfilling the phase conjugation relation are correlated (twin mode 1 and twin mode 2, represented as overlapped colored regions in the near field). After propagation to the far field (FF), those correlated modes are contained in an annulus-shaped region resulting from the phase-matching condition. On this diagram, we only represent the positive- $q_x$  part of twin mode 1 and the correlated negative- $q_x$  part of twin mode 2. These correlated modes follow the  $z$ -axial symmetry imposed by the phase-matching condition, and we further assume that they are contained in RGRs that are on the  $q_x$  axis. In order to create a multi-spatial-mode squeezed field which is fully included in a RGR, i.e., in a simply connected gain region in the far field, one can superpose RGR<sub>2</sub> on RGR<sub>1</sub> on a 50/50 beam splitter (not shown on this diagram) and select  $A_1$  as the new optical axis. This is equivalent to translating the spectrum of the field in RGR<sub>2</sub> by  $q_0$  and the spectrum of the field in RGR<sub>1</sub> by  $-q_0$  along  $q_x$ .



shown in Fig. 4. For the matched RGRs to overlap properly, the magnitude  $q_0$  must lie close to the middle point of the effective gain spectrum (Fig. 3). Redefining the overlapped  $A_1$  and  $A_2$  axes as the main optical axis, the resulting output field is

$$E'(\mathbf{q}, \Omega) = \frac{1}{\sqrt{2}} [E(\mathbf{q} + \mathbf{q}_0, \Omega) + E(\mathbf{q} - \mathbf{q}_0, \Omega)], \quad (1)$$

where the  $x$  coordinate of the redefined  $\mathbf{q}$  is restricted to the region  $[-q_0, q_0]$ . It can be shown (Appendix A) that the output field exhibits far-field correlations that are symmetric with respect to  $\mathbf{q}_0$ , that is to say, with respect to the new optical axis, and that the near-field spatial squeezing spectrum is derived from the gapless effective spectrum. It therefore contains all the spatial frequencies centered on dc and in a bandwidth of the order of  $q_0$ .

At this stage, we have engineered a field with local correlations in the near field, which spans a bandwidth  $\Delta\Omega = 30$  MHz and connects frequency sidebands separated by twice the hyperfine splitting  $2\Omega \approx 6$  GHz. This composite field forms our squeezed signal. A homodyne detector using a single-frequency LO at  $\omega_0$  would reveal the squeezing around an analyzing frequency of approximately 3 GHz. Instead, we use a bichromatic local oscillator (BLO) as proposed by Marino *et al.* [29], where the single-frequency component is replaced by two frequency components, one for each of the probe and conjugate sidebands.

Since each frequency component is resonant with one of the correlated sidebands, the BLO translates the squeezing spectrum from approximately 3 GHz down to dc, and the resulting noise on the photocurrent  $i$  has a similar form to that of quadrature squeezing measured by a monochromatic LO [29]:

$$\langle \Delta i^2 \rangle \propto e^{2s} \cos^2 \left( \frac{\chi_p + \chi_c - \theta_s}{2} \right) + e^{-2s} \sin^2 \left( \frac{\chi_p + \chi_c - \theta_s}{2} \right), \quad (2)$$

where  $\chi_{p,c}$  represents the phase difference between the LO and the signal for the probe and conjugate components, respectively;  $\theta_s$  is the squeezing angle, and  $s$  is the squeezing parameter.

We use a separate 4WM process to generate the required frequency components of the BLO. A seed field at the probe frequency in one RGR stimulates the generation of bright amplified probe and conjugate fields in opposite RGRs. These are superimposed on the overlapping beam splitter to form the BLO (Fig. 5), in a similar manner as for the squeezed signal field. This produces a bright bichromatic beam whose two frequency components tend to propagate along the same axis and have the same mode

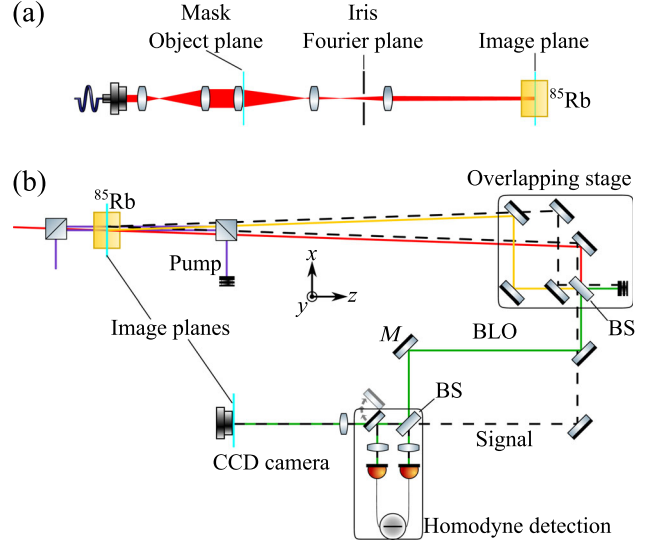


FIG. 5. Schematic diagram of the setup. (a) The path of the seed to the vapor cell, with mask and filtering iris positions. (b) The creation and measurement of the squeezed vacuum. The dashed black lines depict the vacuum fields, which at all points contain both the probe and conjugate frequencies. The solid lines depict bright fields. The red and yellow lines represent probe and conjugate LO frequencies, respectively. The green line represents the BLO, the purple the pump field. The cyan lines show the mask object and image positions. Where the vacuum and LO fields are slightly offset in the diagram, they are actually separated vertically in the experiment. Nonetheless, we use a single beam splitter (BS) for both of them in the overlapping stage.

shape in the near field. We will see in Sec. VB that this field has the right properties for the BLO.

#### IV. EXPERIMENTAL SETUP

A simplified experimental setup is shown in Fig. 5. A single heated rubidium cell is pumped by a pair of parallel pump beams, thus producing two nonoverlapping 4WM amplifiers. A set of mirrors and a beam splitter overlap a pair of matched RGRs as in Fig. 4. This operation is realized for both 4WM amplifiers. To generate the BLO, we seed one of the amplifiers, at the probe frequency, with a mode that is contained within one of the RGRs. The other amplifier is left unseeded to generate the signal field. The resulting BLO and signal fields are fed into a homodyne detector to measure the noise on the signal.

The relative phase between the signal and LO fields, which controls the measured signal quadrature, is tuned by adjusting the optical path length of the BLO with a piezoelectric actuator. Using this method, we have generated squeezing levels of up to 3.6 dB as shown in Fig. 6.

Since our main experimental aim is to investigate the local character of the quantum correlations, we need to shape the BLO in the near field identically for both frequency components. This is achieved by shaping the

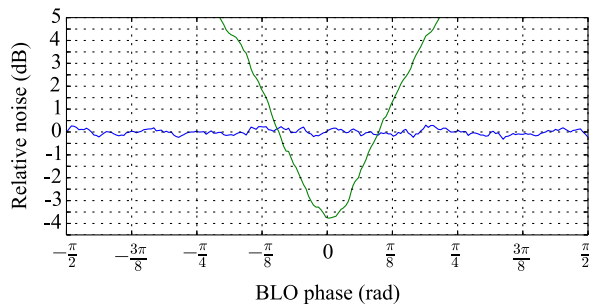


FIG. 6. Typical squeezing graph, generated by scanning the phase difference between BLO and signal fields. For this data, the LO pump power is 900 mW, the signal pump power is 950 mW, and the gain is around 4. The electronic noise floor can also be subtracted, revealing a squeezing level of 3.8 dB.

seed with a mask which is optically conjugated with the gain medium [Fig. 5(a)]. High spatial frequencies, introduced by the mask, are filtered out with an aperture located in the Fourier plane. In the same way, the position of the BLO in the near field is controlled by steering the seed beam before the cell. The actual mode shape and position of the BLO can be recorded with an imaging lens located after the overlapping beam splitter. More experimental details can be found in Appendix B.

## V. RESULTS

### A. Multimode squeezing

At this stage, we have a MSM quadrature-squeezed field, which should present local quadrature squeezing, and a LO capable of analyzing it. The steps described above to produce this field are required to remedy issues specific to our 4WM process, namely, the existence of gaps in the spatial and frequency spectra of the gain. Beyond this apparent complexity, the local squeezing is the usual consequence of the creation of local correlations inside the amplifying medium. The signal field and BLO can be used to realize the simple experiment described in Fig. 1; that is to say, they can display squeezing in a homodyne detector arrangement for an arbitrary transverse position of the BLO.

We want to show the local character of the squeezing on two perpendicular directions, completing the measurement on one direction at a time. To this effect, we reduce the size of the BLO mode along the direction of interest, using a slit as the mask, while allowing the BLO mode to retain its full extent in the perpendicular direction.

The near-field BLO mode shape and the signal quadrature squeezing are recorded as the BLO is moved across the near field in the direction of its narrow size, while keeping its direction of propagation constant. A Gaussian fit of the BLO profile gives both its size, which remains constant, and position. Figure 7 shows the degree of squeezing as a function of the position of the BLO. The

green squares and Figs. 7(b) and 7(e) show the squeezing using a gain of around 4. They clearly demonstrate local squeezing over a wide range of nonoverlapping positions of the BLO in both directions and thus the highly MSM nature of the system.

So far, we have assumed a thin medium at  $z = 0$ ; in practice, the cell has a finite length of 12.5 mm, and propagation effects cannot be fully neglected. A mode of very small transverse size will inevitably diffract over the length of the gain medium, and as a result, the correlations cannot be fully local. This gives rise to a minimum area

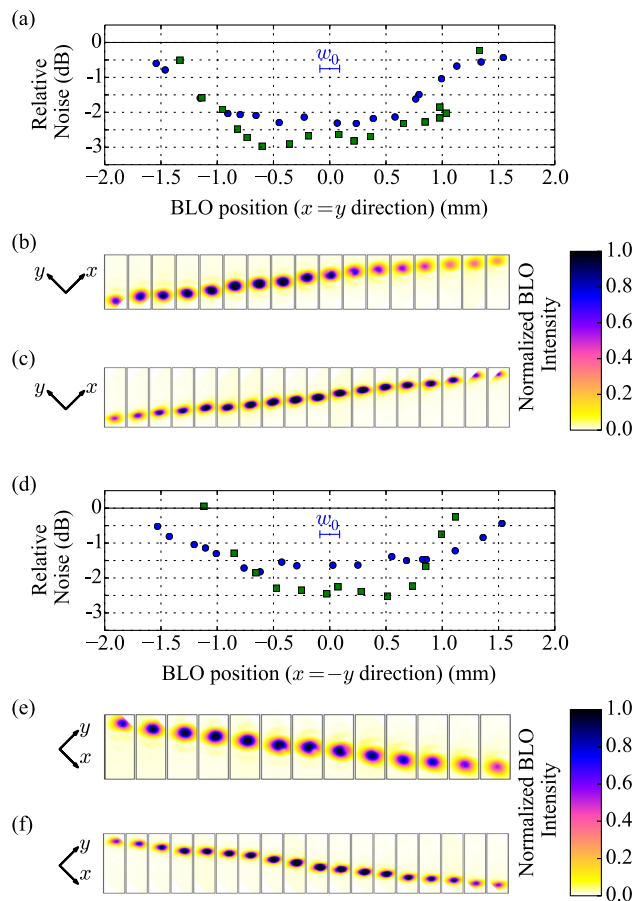


FIG. 7. Local multimode squeezing. (a) Squeezing as a function of BLO position. The BLO position is extracted from (b) and (c), which show images of the BLO as it is translated along the  $x = y$  direction. The series of images in (b) (wider BLO) corresponds to the green squares. Series (c) (narrower BLO) corresponds to the blue circles. (d) Squeezing as a function of BLO position as it is translated along the  $x = -y$  direction; again, (e) and (f) show the images corresponding to the green and blue data, respectively. The black lines indicate the QNL, and the green squares show the data for parameters resulting in a gain of 4, with BLO mode waist dimensions of  $0.45 \text{ mm} \times 0.61 \text{ mm}$ , and the blue circles show the data for parameters resulting in a gain of 2, with BLO mode waist dimensions of  $0.31 \text{ mm} \times 0.58 \text{ mm}$ . All the results are corrected for the electronic noise floor (at  $-13 \text{ dB}$ ). The scale bar labeled  $w_0$  indicates the size of the coherence area, extracted from Fig. 8.

over which local squeezing can be observed, referred to as the coherence area, and a corresponding coherence length [30]. In the above results, we have used a BLO with its smaller dimension chosen such that a reasonable level of squeezing remains. In the blue circles and Figs. 7(c) and 7(f), the gain is reduced to around 2 and squeezing can be observed for a smaller slit width, and over a larger range of positions, albeit at a lower level. More generally, the impact of the slit size on the squeezing level can be seen in Fig. 8. There is a small size  $w_0 = 0.18$  mm of the BLO for which local squeezing can still be observed. This point is reached when the diffracted far-field size of the BLO in the same transverse direction occupies the whole RGR.

We extract from Fig. 7 the size of the squeezing region  $l = 3.1$  mm in both the  $x = y$  and  $x = -y$  directions. Taking  $w_0$  to be the coherence length, one gets a total number of squeezed modes  $l^2/4w_0^2 = 75$ .

The measured coherence length can also be compared to the theoretical value of the coherence length as described by Lopez *et al.* [13]. It is the waist of a beam such that the Rayleigh range is equal to the length of the gain medium, and is given by

$$l_{\text{coh}} = \sqrt{\frac{\lambda l_g}{\pi n_s}}, \quad (3)$$

where  $n_s$  is the refractive index and is taken to be 1,  $\lambda$  is the wavelength, and  $l_g$  is the length of the gain medium, in this case the rubidium cell. With the parameters in our system, the theoretical coherence length is  $l_{\text{coh}} = 0.056$  mm. The corresponding number of squeezed modes  $N$  is then calculated by comparing the pump waist  $w_p$  and the coherence length:

$$N = \frac{w_p^2}{l_{\text{coh}}^2}. \quad (4)$$

With our parameters, this expression leads to an estimate of 300 independent modes being squeezed. However, in our experiment, we only collect and analyze a small portion of the 4WM emission annulus (see Fig. 4) and thus only have access to a fraction of these modes.

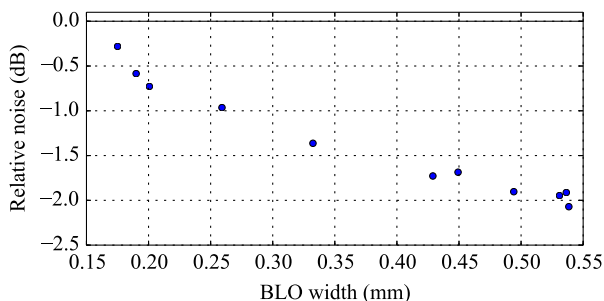


FIG. 8. Quantum-noise reduction as a function of the width of the BLO.

The maximum number of squeezed modes could be increased by enlarging the pump beam. Alternatively, the same effect could be achieved by reducing the coherence length, which is done by reducing the length of the gain medium. Both of these adjustments would require the medium to be pumped with a higher power in order to attain the same gain.

It can be seen from Fig. 4 that the RGRs, as they are formed, have different  $x$  and  $y$  dimensions. We have checked that this results in a significant difference in the number of modes between the  $x$  and  $y$  directions.

## B. Structure of the LO

It is clear from the results above that the squeezed field is spatially multimode and the BLO can have an arbitrary shape, as long as its spatial spectrum fits in the spatial bandwidth of the 4WM process. However, in order to measure squeezing, the probe and conjugate components of the BLO must follow the phase conjugation dictated by the 4WM. Classically, for a flat pump wavefront, this conjugation reads  $E_p(\mathbf{\rho}) = E_c^*(\mathbf{\rho})$  for all  $\mathbf{\rho}$  in the near-field plane. Although this seems a rather straightforward condition to fulfil, it should be noted that not matching the BLO to the spatial structure of the squeezed vacuum leads to a rapid loss of measured squeezing [31]. Indeed, squeezing measurements of multimode fields are sensitive to LO wavefront distortions. Any imperfection in the LO phase profile causes antisqueezed quadratures of higher-order spatial modes to be measured alongside the squeezed quadrature of the target mode, resulting in a noise level which is typically above the QNL.

A possible solution to this experimental difficulty is to use the nonlinear process itself to create the LO bright field [25,32]. We implement this method by stimulating the second 4WM process to generate bright probe and conjugate fields that can be used to form the BLO (Fig. 5). Provided both pumps have the same mode shape, the BLO automatically matches the structure of the squeezed vacuum, both in phase and amplitude, irrespective of the chosen pump mode and the associated phase conjugation. Note that we still need to accurately overlay the very same RGRs for both the BLO and the signal.

In spite of the strong constraints on the wavefront of the LO, it was suggested [22] that spatially multimode squeezing can improve the detection of quantum-noise reduction due to the relaxed constraints on the LO shape. We could indeed verify that the measured squeezing was only mildly dependent on the overlap of the BLO with the signal in the homodyne detector (e.g., tuning of mirror  $M$  in Fig. 5).

## C. Experimental limitations

There are a number of reasons why a finite amount of squeezing can be observed, well below the theoretical value dictated by the gain. The main one comes from the way the

BLO is generated. Seeding at only the probe frequency induces a power imbalance between the probe and conjugate frequency components in the BLO, resulting in an uneven detection of the correlated sidebands. Increasing the gain reduces this imbalance but increases the antisqueezing in the signal, making the squeezing measurements more sensitive to misalignment, as explained in the previous section. This tradeoff sets the optimum gain value in the range of 2–4. The squeezing is also limited by other imperfections affecting the reflectance of the mirrors, the transmittance of the antireflection coatings, and the quantum efficiency of the detectors.

Throughout this experiment, we have chosen to work in the near field where the local correlations between probe and conjugate frequency components are generated. It is possible to transfer these local correlations to the far field. Because of the theoretical axial symmetry of the correlations in the far field, a flip of one of the RGRs in each of the  $q_x$  and  $q_y$  directions is required (see Fig. 4). In practice, the probe and conjugate propagate differently due to the Kerr lensing of the probe in the medium, and correlated probe and conjugate modes in the far field have slightly different shapes [25]. If one is not concerned with accurate control of the LO shape, or sharply localized squeezing, then it is still possible to observe multimode squeezing in this fashion. Indeed, we have successfully measured squeezing up to 2 dB in this arrangement, with results limited by the additional experimental complexity.

## VI. CONCLUSION

We have demonstrated the generation of a light field which displays local squeezing in a total of 75 independent modes using a 4WM system in a hot rubidium vapor. The squeezing exists as quantum correlations between distant frequency sidebands; however, our setup provides a natural way to generate the arbitrarily shaped bichromatic local oscillator required to measure the multi-spatial-mode squeezing.

Such a quantum state of light can theoretically be used to improve super-resolution techniques [9], when overlapped with a bright optical carrier to form a bright illumination. In future work, and as a step toward quantum-enhanced super-resolution, we are aiming to demonstrate local intensity quantum-noise reduction of the resulting illumination in the temporal domain. Directly imaging the light with a camera in a series of snapshots should reveal local intensity fluctuations below the shot noise in arbitrary regions of the images.

## ACKNOWLEDGMENTS

This research was supported by the Engineering and Physical Sciences Research Council Grants No. EP/E036473/1 and No. EP/I001743/1.

## APPENDIX A: CORRELATION PROPAGATION

Let us consider the electromagnetic field at the frequency sidebands  $\pm\Omega$  propagating along the  $z$  axis. In a perpendicular plane, taken to be the near field at  $z = 0$ , the field operator  $E(\boldsymbol{\rho}, \Omega)$  can be decomposed on the local quadrature operators, themselves expressed as local creation and annihilation operators:

$$X(\boldsymbol{\rho}, \Omega) = \frac{1}{2}[a^\dagger(\boldsymbol{\rho}, \Omega) + a(\boldsymbol{\rho}, \Omega)], \quad (\text{A1})$$

$$Y(\boldsymbol{\rho}, \Omega) = \frac{i}{2}[a^\dagger(\boldsymbol{\rho}, \Omega) - a(\boldsymbol{\rho}, \Omega)], \quad (\text{A2})$$

where  $\boldsymbol{\rho}$  is the transverse position. The same relations hold in momentum space, and equivalently, due to Fraunhofer diffraction, in the far field at  $z = \infty$ , the field  $E(\mathbf{q}, \Omega)$  can be decomposed on

$$X(\mathbf{q}, \Omega) = \frac{1}{2}[a^\dagger(\mathbf{q}, \Omega) + a(\mathbf{q}, \Omega)], \quad (\text{A3})$$

$$Y(\mathbf{q}, \Omega) = \frac{i}{2}[a^\dagger(\mathbf{q}, \Omega) - a(\mathbf{q}, \Omega)], \quad (\text{A4})$$

where  $a(\mathbf{q}, \Omega)$  is the spatial Fourier transform of  $a(\boldsymbol{\rho}, \Omega)$  and  $a^\dagger(\mathbf{q}, \Omega)$  is the adjoint of  $a(\mathbf{q}, \Omega)$ . Note that  $a^\dagger(\mathbf{q}, \Omega)$  is also the Fourier transform of  $a^\dagger(-\boldsymbol{\rho}, \Omega)$ . In effect, this means that  $X(\mathbf{q}, \Omega)$  is not the Fourier transform of  $X(\boldsymbol{\rho}, \Omega)$ . Physically, this property reflects the phase-matching condition, and as we will now see, it transforms local correlations in the near field into symmetric correlations between  $\mathbf{q}$  and  $-\mathbf{q}$  in the far field.

A thin nonlinear medium at  $z = 0$ , where propagation and the associated diffraction can be neglected, creates local correlations which depend on the local phase of the pump field. For instance, for a pump with a infinite flat wavefront (i.e., with a well-defined wave vector  $\mathbf{k}_0$ ), the following two joint quadratures are squeezed for all  $\boldsymbol{\rho}$ :

$$X_-(\boldsymbol{\rho}, \Omega) = \frac{1}{\sqrt{2}}[X(\boldsymbol{\rho}, \Omega) - X(\boldsymbol{\rho}, -\Omega)], \quad (\text{A5})$$

$$Y_+(\boldsymbol{\rho}, \Omega) = \frac{1}{\sqrt{2}}[Y(\boldsymbol{\rho}, \Omega) + Y(\boldsymbol{\rho}, -\Omega)]. \quad (\text{A6})$$

In the far field, one can form another joint quadrature and express it as a function of  $X_-(\boldsymbol{\rho}, \Omega)$  and  $Y_+(\boldsymbol{\rho}, \Omega)$ :



$$\begin{aligned}
X_-(\mathbf{q}, \Omega) &= \frac{1}{\sqrt{2}} [X(\mathbf{q}, \Omega) - X(-\mathbf{q}, -\Omega)] \\
&= \frac{1}{2\sqrt{2}} [a^\dagger(\mathbf{q}, \Omega) + a(\mathbf{q}, \Omega) \\
&\quad - a^\dagger(-\mathbf{q}, -\Omega) - a(-\mathbf{q}, -\Omega)] \\
&= \frac{1}{2\sqrt{2}} \mathcal{F}[a^\dagger(-\boldsymbol{\rho}, \Omega) \\
&\quad + a(\boldsymbol{\rho}, \Omega) - a^\dagger(\boldsymbol{\rho}, -\Omega) - a(-\boldsymbol{\rho}, -\Omega)] \\
&= \frac{1}{\sqrt{2}} \mathcal{F}[X_-(\boldsymbol{\rho}, \Omega) + X_-(\boldsymbol{\rho}, \Omega)], \quad (\text{A7})
\end{aligned}$$

where  $\mathcal{F}$  is the Fourier transform operation. Since  $X_-(\boldsymbol{\rho}, \Omega)$  is squeezed for all  $\boldsymbol{\rho}$ , then so is  $X_-(\mathbf{q}, \Omega)$  for all  $\mathbf{q}$ . In a similar fashion, one can show that the same result applies to

$$Y_+(\mathbf{q}, \Omega) = \frac{1}{\sqrt{2}} [Y(\mathbf{q}, \Omega) + Y(-\mathbf{q}, -\Omega)]. \quad (\text{A8})$$

This implies that the fields at positions  $\pm\mathbf{q}$  are entangled [33]. Reference [30] gives an account of the near- and far-field correlations for the intensity.

We now show that the overlapping operation shown in Fig. 4 preserves the local correlations in the near field while restricting the accessible spatial spectrum of the fluctuations to the positive side. By overlapping two opposite RGRs of the emission annulus in the far field, one translates the fields transversely by  $\pm\mathbf{q}_0$ . As a result, the creation operator transforms as

$$a'(\mathbf{q}, \Omega) = \frac{1}{\sqrt{2}} [a(\mathbf{q} - \mathbf{q}_0, \Omega) + a(\mathbf{q} + \mathbf{q}_0, \Omega)], \quad (\text{A9})$$

with  $q_x \in [-q_0, q_0]$ . The phase of the superposition is arbitrary and has no bearing on the final conclusion. According to Eqs. (A8) and (A7), the entanglement occurs between opposite sidebands  $\pm\Omega$  and opposite transverse wave vectors  $\pm\mathbf{q}$ . For now, we restrict ourselves to a particular pair of correlated sidebands, where the  $\Omega$  sideband comes from the left RGR and the  $-\Omega$  sideband comes from the right RGR. Within this simplification, the creation operator is

$$a'(\mathbf{q}, \pm\Omega) = a(\mathbf{q} \pm \mathbf{q}_0, \pm\Omega) \quad (\text{A10})$$

or equivalently, in the near field,

$$a'(\boldsymbol{\rho}, \pm\Omega) = a(\boldsymbol{\rho}, \pm\Omega) e^{\mp i\varphi}, \quad (\text{A11})$$

with  $\varphi = \mathbf{q}_0 \cdot \boldsymbol{\rho}$ . From this, we can derive the following quadrature transformations:

$$X'(\boldsymbol{\rho}, \pm\Omega) = X(\boldsymbol{\rho}, \pm\Omega) \cos \varphi + Y(\boldsymbol{\rho}, \pm\Omega) \sin \varphi, \quad (\text{A12})$$

$$Y'(\boldsymbol{\rho}, \pm\Omega) = Y(\boldsymbol{\rho}, \pm\Omega) \cos \varphi - X(\boldsymbol{\rho}, \pm\Omega) \sin \varphi. \quad (\text{A13})$$

and directly, we get

$$X'_-(\boldsymbol{\rho}, \Omega) = X_-(\boldsymbol{\rho}, \Omega) \cos \varphi - Y_+(\boldsymbol{\rho}, \Omega) \sin \varphi, \quad (\text{A14})$$

$$Y'_+(\boldsymbol{\rho}, \Omega) = X_-(\boldsymbol{\rho}, \Omega) \sin \varphi + Y_+(\boldsymbol{\rho}, \Omega) \cos \varphi. \quad (\text{A15})$$

Since the joint quadratures  $X_-(\boldsymbol{\rho}, \Omega)$  and  $Y_+(\boldsymbol{\rho}, \Omega)$  are locally squeezed, this is also the case for the output joint quadratures  $X'_-(\boldsymbol{\rho}, \Omega)$  and  $Y'_+(\boldsymbol{\rho}, \Omega)$ . The output field also has a contribution from the other possible configuration, where the  $\Omega$  sideband comes from the right RGR and the  $-\Omega$  sideband comes from the left RGR. This contribution has output joint quadratures that are similar to those given in Eqs. (A14) and (A15). Both contributions are uncorrelated, and their noises add in quadrature, so that their superposition is also squeezed. As a result, the output field displays the same local squeezing as the field inside the nonlinear medium, while having a continuous spatial spectrum centered on 0 for both the  $x$  and  $y$  directions.

We have considered here a medium of zero length, which results in perfectly localized squeezing. In practice, the cell has a finite length, which gives rise to a finite minimum size of a squeezed area, called coherence length. This is studied in Sec. VA.

## APPENDIX B: EXPERIMENTAL DETAILS

To ensure relative phase stability, all laser beams are derived from a single Ti: sapphire laser, tuned approximately 800 MHz from the  $5^2S_{1/2}(F=2) \rightarrow 5^2P_{1/2}$  atomic transition at 795 nm. The main laser beam is split, with two equal parts being used for the LO pump and the signal pump at 900 mW, and a final small portion being used to generate the seed beam at the probe frequency. To do this, an acousto-optic modulator (AOM) is operated at 1.520 GHz in a double-pass arrangement. The seed beam has a power of 130  $\mu\text{W}$ . It is amplified by the 4WM, with a gain of around 4 with our parameters, and is used to generate a BLO with a total power of up to 910  $\mu\text{W}$ . The pump beam has a waist of 1 mm in the center of the cell, while the unvignetted seed beam has a waist of 0.35 mm. All of the noise signals are measured with a spectrum analyzer using a detection frequency of 1 MHz, a resolution bandwidth of 100 kHz, and a video bandwidth of 30 Hz. To obtain the largest possible squeezing spatial bandwidth, the parameters are tweaked such that the BLO pump power is 1.3 W, the signal pump power is 580 mW, and the AOM is operated at 1.523 GHz. This leads to a gain of around 2 and a final BLO power of 215  $\mu\text{W}$ .

A 12.5-mm-long rubidium vapor cell, heated to approximately 120°C, forms the gain medium. The cell is contained within a vacuum chamber to avoid the convection air currents around the heat pipe and hence eliminate wavefront distortions due to refractive index fluctuations on the signal and BLO optical paths.

The production of quadrature squeezing on the overlapping beam splitter occurs only when the phase difference between the two RGRs at the beam splitter is the same for both the probe and the conjugate. We ensure this condition by adjusting the difference in the optical path of the two RGRs from the cell to the overlapping beam splitter to an inaccuracy much smaller than the beat length between the probe and the conjugate (5 cm, corresponding to a frequency difference of  $\omega_c - \omega_p = 6$  GHz). To achieve this, we temporarily seed the signal 4WM process symmetrically with one seed in each RGR and use the visibility of the resulting bichromatic interference on the overlapping beam splitter to minimize the path length difference. Typically, a visibility of 99% can be achieved. Similarly, to ensure a good overlap between the two frequency components of the LO, we use independent interferences between each of the components of the LO and the corresponding component of the previously aligned seeded signal modes.

To control the size of the BLO in the direction of interest, we clip the seed with a slit made up of two razor blades. The sharp edges of the slit introduce high-order spatial modes, with large  $|\mathbf{q}|$ , lying outside of the spatial gain profile. These high-order modes will only be present in the probe frequency component. A filtering iris is placed in the Fourier plane to remove these spatial frequencies before the 4WM cell. The iris size is adjusted to cut at the first zero in the Fourier spectrum.

In order to be able to measure the squeezing using the homodyne detection and also image the BLO modes on a camera, a flip mirror is used to control the direction of the beam incident on one side of the balanced detector. A single lens images the near-field gain region on the camera.

---

[1] V. Giovannetti, S. Lloyd, and L. Maccone, *Quantum-Enhanced Measurements: Beating the Standard Quantum Limit*, *Science* **306**, 1330 (2004).  
 [2] M. I. Kolobov, *Quantum Imaging* (Springer, New York, 2006).  
 [3] G. Brida, M. Genovese, and I. R. Berchera, *Experimental Realization of Sub-Shot-Noise Quantum Imaging*, *Nat. Photonics* **4**, 227 (2010).  
 [4] T. Ono, R. Okamoto, and S. Takeuchi, *An Entanglement-Enhanced Microscope*, *Nat. Commun.* **4**, 2426 (2013).  
 [5] Y. Israel, S. Rosen, and Y. Silberberg, *Supersensitive Polarization Microscopy Using NOON States of Light*, *Phys. Rev. Lett.* **112**, 103604 (2014).  
 [6] L. A. Rozema, J. D. Bateman, D. H. Mahler, R. Okamoto, A. Feizpour, A. Hayat, and A. M. Steinberg, *Scalable Spatial Superresolution Using Entangled Photons*, *Phys. Rev. Lett.* **112**, 223602 (2014).  
 [7] M. A. Taylor, J. Janousek, V. Daria, J. Knittel, B. Hage, H.-A. Bachor, and W. P. Bowen, *Biological Measurement beyond the Quantum Limit*, *Nat. Photonics* **7**, 229 (2013).  
 [8] M. A. Taylor, J. Janousek, V. Daria, J. Knittel, B. Hage, H.-A. Bachor, and W. P. Bowen, *Subdiffraction-Limited*

*Quantum Imaging within a Living Cell*, *Phys. Rev. X* **4**, 011017 (2014).  
 [9] M. I. Kolobov and C. Fabre, *Quantum Limits on Optical Resolution*, *Phys. Rev. Lett.* **85**, 3789 (2000).  
 [10] M. Pysher, Y. Miwa, R. Shahrokshahi, R. Bloomer, and O. Pfister, *Parallel Generation of Quadripartite Cluster Entanglement in the Optical Frequency Comb*, *Phys. Rev. Lett.* **107**, 030505 (2011).  
 [11] J. Roslund, R. Medeiros de Araujo, S. Jiang, C. Fabre, and N. Treps, *Wavelength-Multiplexed Quantum Networks with Ultrafast Frequency Combs*, *Nat. Photonics* **8**, 109 (2014).  
 [12] M. I. Kolobov and I. V. Sokolov, *Spatial Behavior of Squeezed States of Light and Quantum Noise in Optical Images*, *Sov. Phys. JETP* **69**, 1097 (1989).  
 [13] L. Lopez, B. Chalopin, A. Riviere de la Souhre, C. Fabre, A. Matre, and N. Treps, *Multimode Quantum Properties of a Self-Imaging Optical Parametric Oscillator: Squeezed Vacuum and Einstein-Podolsky-Rosen-Beams Generation*, *Phys. Rev. A* **80**, 043816 (2009).  
 [14] B. Chalopin, F. Scazza, C. Fabre, and N. Treps, *Direct Generation of a Multi-transverse Mode Non-classical State of Light*, *Opt. Express* **19**, 4405 (2011).  
 [15] O. Jedrkiewicz, Y.-K. Jiang, E. Brambilla, A. Gatti, M. Bache, L. A. Lugiato, and P. Di Trapani, *Detection of Sub-Shot-Noise Spatial Correlation in High-Gain Parametric Down Conversion*, *Phys. Rev. Lett.* **93**, 243601 (2004).  
 [16] E. Brambilla, L. Caspani, O. Jedrkiewicz, L. A. Lugiato, and A. Gatti, *High-Sensitivity Imaging with Multi-mode Twin Beams*, *Phys. Rev. A* **77**, 053807 (2008).  
 [17] I. N. Agafonov, M. V. Chekhova, and G. Leuchs, *Two-Color Bright Squeezed Vacuum*, *Phys. Rev. A* **82**, 011801 (2010).  
 [18] N. Treps, N. Grosse, W. P. Bowen, C. Fabre, H.-A. Bachor, and P. K. Lam, *A Quantum Laser Pointer*, *Science* **301**, 940 (2003).  
 [19] V. Boyer, A. M. Marino, and P. D. Lett, *Generation of Spatially Broadband Twin Beams for Quantum Imaging*, *Phys. Rev. Lett.* **100**, 143601 (2008).  
 [20] N. Corzo, A. M. Marino, K. M. Jones, and P. D. Lett, *Multi-Spatial-Mode Single-Beam Quadrature Squeezed States of Light from Four-Wave Mixing in Hot Rubidium Vapor*, *Opt. Express* **19**, 21358 (2011).  
 [21] R. E. Slusher, L. W. Hollberg, B. Yurke, J. C. Mertz, and J. F. Valley, *Observation of Squeezed States Generated by Four-Wave Mixing in an Optical Cavity*, *Phys. Rev. Lett.* **55**, 2409 (1985).  
 [22] L. A. Lugiato and Ph. Grangier, *Improving Quantum-Noise Reduction with Spatially Multimode Squeezed Light*, *J. Opt. Soc. Am. B* **14**, 225 (1997).  
 [23] R. W. Boyd, *Nonlinear Optics*, 3rd ed. (Academic, Amsterdam, 2008).  
 [24] C. F. McCormick, V. Boyer, E. Arimondo, and P. D. Lett, *Strong Relative Intensity Squeezing by Four-Wave Mixing in Rubidium Vapor*, *Opt. Lett.* **32**, 178 (2007).  
 [25] V. Boyer, A. M. Marino, R. C. Pooser, and P. D. Lett, *Entangled Images from Four-Wave Mixing*, *Science* **321**, 544 (2008).  
 [26] N. V. Corzo, A. M. Marino, K. M. Jones, and P. D. Lett, *Noiseless Optical Amplifier Operating on Hundreds of Spatial Modes*, *Phys. Rev. Lett.* **109**, 043602 (2012).

- [27] P. Kumar and M. I. Kolobov, *Degenerate Four-Wave Mixing as a Source for Spatially-Broadband Squeezed Light*, *Opt. Commun.* **104**, 374 (1994).
- [28] M. T. Turnbull, P. G. Petrov, C. S. Embrey, A. M. Marino, and V. Boyer, *Role of the Phase-Matching Condition in Nondegenerate Four-Wave Mixing in Hot Vapors for the Generation of Squeezed States of Light*, *Phys. Rev. A* **88**, 033845 (2013).
- [29] A. M. Marino, Jr., C. R. Stroud, V. Wong, R. S. Bennink, and R. W. Boyd, *Bichromatic Local Oscillator for Detection of Two-Mode Squeezed States of Light*, *J. Opt. Soc. Am. B* **24**, 335 (2007).
- [30] E. Brambilla, A. Gatti, M. Bache, and L. A. Lugiato, *Simultaneous Near-Field and Far-Field Spatial Quantum Correlations in the High-Gain Regime of Parametric Down-Conversion*, *Phys. Rev. A* **69**, 023802 (2004).
- [31] A. La Porta and R. E. Slusher, *Squeezing Limits at High Parametric Gains*, *Phys. Rev. A* **44**, 2013 (1991).
- [32] C. Kim and P. Kumar, *Quadrature-Squeezed Light Detection Using a Self-Generated Matched Local Oscillator*, *Phys. Rev. Lett.* **73**, 1605 (1994).
- [33] L.-M. Duan, G. Giedke, J. I. Cirac, and P. Zoller, *Inseparability Criterion for Continuous Variable Systems*, *Phys. Rev. Lett.* **84**, 2722 (2000).